Biochemical and Biophysical Research Communications 423 (2012) 319–324

Contents lists available at SciVerse ScienceDirect

Biochemical and Biophysical Research Communications

journal homepage: www.elsevier.com/locate/ybbrc

A molecular dynamics investigation on the crizotinib resistance mechanism of C1156Y mutation in ALK

Hui-Yong Sun [a], Feng-Qin Ji [b,c,*]

[a] Shandong University of Technology, Zibo 255049, PR China
[b] National Key Laboratory of Crop Genetic Improvement, College of Life Science and Technology, Huazhong Agricultural University, Wuhan 430070, PR China
[c] Center for Bioinformatics, Huazhong Agricultural University, Wuhan 430070, PR China

ARTICLE INFO

Article history:
Received 17 May 2012
Available online 30 May 2012

Keywords:
EML4-ALK
Mutation
Crizotinib
Resistance mechanism
Molecular dynamics

ABSTRACT

Crizotinib is an anaplastic lymphoma kinase (ALK) inhibitor that has recently been approved in the US for the treatment of non-small cell lung carcinoma (NSCLC). Despite its outstanding safety and efficacy, several resistant mutations against crizotinib have been detected in the treatment of NSCLC. However, in contrast to the widely accepted mechanism of steric hindrance by mutations at the active site, the mechanism by which the C1156Y non-active site mutation confers resistance against crizotinib remains unclear. In the present study, the resistance mechanism of C1156Y in ALK was investigated using molecular dynamics simulations. The results suggest that despite the non-active site mutation, C1156Y causes the dislocation of crizotinib as well as the indirect conformational changes in the binding cavity, which results in a marked decrease in the van der Waals and electrostatic interactions between crizotinib and ALK. The obtained results provide a detailed explanation of the resistance caused by C1156Y and may give a vital clue for the design of drugs to combat crizotinib resistance.

1. Introduction

Echinoderm microtubule-associated protein-like 4 (EML4)-anaplastic lymphoma kinase (ALK) is a fusion-type protein tyrosine kinase produced through gene rearrangement [1]. Despite its occurrence in only 3–7% of non-small cell lung carcinoma (NSCLC) patients, its total number of cases is larger than those of several other malignancies [2]. In 2007, EML4–ALK was first identified as a potential molecular target in NSCLC [3]. Recently, the Food and Drug Administration has approved crizotinib, an oral small-molecule inhibitor of ALK, for the treatment of NSCLCs with positive ALK gene rearrangement. Thus, crizotinib became the first new drug approved for lung cancer in the past six years. Given its excellent activity, an editor of the New England Journal of Medicine praised crizotinib as "a new champion in the cancer war" [4].

Unfortunately, cancers have eventually developed resistance to crizotinib. In 2010, Choi et al. [5] identified two secondary mutations (C1156Y and L1196M) within the kinase domain of EML4-ALK, which confer marked crizotinib resistance. In contrast to the gatekeeper mutation L1196M, which confers resistance to crizotinib through the steric hindrance of drug binding, the resistance mechanism of C1156Y at the non-active N-terminal domain is unknown. Recently, Shen et al. [6] proposed a mechanism of C1156Y resistance using molecular docking. They suggested that the C1156Y mutation induces conformational changes in the loop 1122–1130 fragment and speculated that C1156Y-based resistance results from the decreased binding affinity of crizotinib. This viewpoint provides a new insight into crizotinib resistance. In the current study, the C1156Y-based mechanism of crizotinib resistance was investigated in detail through molecular dynamics (MD), calculation of MM/GBSA free energy, and residue decomposition. The results show that the C1156Y mutation causes a displacement of crizotinib as well as conformational changes in the binding cavity. These changes in turn decrease the interactions with active-site residues and, eventually result in drug resistance.

2. Material and methods

The X-ray crystal structure of ALK in complex with crizotinib (PDB code: 2XP2) was used as the initial structure [7]. The missing residues H1124–G1125, G1137–S1143, P1218–S1219, and S1281–A1289 were modeled using the SYBYL X1.2 program. The initial conformation of crizotinib was exacted from the 2XP2 pdb file. The C1156Y mutation was subsequently introduced into the wild-type (WT) ligand-protein complex using the Biopolymer module of the SYBYL-X1.2 package.

* Corresponding author at: National Key Laboratory of Crop Genetic Improvement, College of Life Science and Technology, Huazhong Agricultural University, Wuhan 430070, PR China. Fax: +86 27 87280877.
E-mail address: fengqinji@mail.hzau.edu.cn (F.-Q. Ji).

0006-291X/$ - see front matter © 2012 Elsevier Inc. All rights reserved.
http://dx.doi.org/10.1016/j.bbrc.2012.05.120

Electrostatic potentials were generated at the Hartree-Fock level with 6-31G* basis set using the Gaussian 03 program [8]. The partial atomic charges for crizotinib were calculated by the RESP fitting method [9]. Amber99SB force field and general AMBER force field (gaff) [10,11] were applied to establish the potentials of ALK and crizotinib respectively. Na^+ counterions were added to neutralize the system. The WT and mutant complexes were then immersed in an 8 Å radius of the TIP3P water model [12].

In the molecular minimization and MD simulations, the particle mesh Ewald (PME) was employed to treat the long-range electrostatic interactions [13]. The five-minimization steps were performed prior to the MD simulations. Initially, movement was allowed only for hydrogen atoms. Afterward, water molecules and ions were allowed to move. Eventually, the side chains were permitted to move freely. Furthermore, the ligand and the main-chain atoms within 5 Å of the mutated residue were minimized. Finally, all atoms were allowed to move freely.

The MD simulations were performed using NAMD (Not Another Molecular Dynamics) program [14]. A 10 Å cutoff was used for the long-rang electrostatic interactions. The covalent bonds involving hydrogen atoms were constrained using the SHAKE algorithm [15]. The time step was set to 2.0 fs. The system was gradually heated with the main chains constrained by 5 kcal/mol Å in the NVT ensemble from 0 to 310 K. About 13 ns equilibrating calculation was executed at 1 atm and at 310 K using the NPT ensemble. The atom coordinates were collected at the interval of 5 ps for the last 10 ns to analyze the structures in detail.

The principal component analysis (PCA), as well as the root-mean-square deviation (RMSD), root mean square fluctuation (RMSF), and hydrogen bond analyses, was performed using NAMD. The average conformations were generated over the last 10 ns of the MD trajectories. The calculation for the dynamic cross correlation (DCC) map was performed on the trajectories using Perl Script.

The binding free energy was calculated using the MM/GBSA procedure. The modified GB model was used to calculate the solvation energy terms [16]. The binding free energy of a protein-ligand complex (ΔG_{bind}) is obtained by the following equations:

$$\Delta G = G_{\mathrm{cpx}} - (G_{rec} + G_{lig})$$

$$G_{bind} = E_{MM} - TS + G_{solv}$$

$$E_{MM} = E_{int} + E_{elec} + E_{vdW}$$

$$G_{solv} = G_{elec,solv} + G_{nonpolar,solv}$$

$$G_{nonpolar,solv} = \gamma A + b$$

where E_{int} includes the bond, angle, and torsional angle energies; E_{elec} and E_{vdW} are the intermolecular electrostatic and van der Waals (vdW) energies, respectively. Therefore, E_{MM} is associated with the enthalpic changes in the gas phase upon binding. G_{solv} is composed of the electrostatic $G_{elec,solv}$ and the nonpolar $G_{nonpolar,solv}$ contributions to solvation. Where A is the solvent-accessible surface area and the solvation parameters; γ and b, were 0.0072 kcal/mol·Å and 0 respectively.

The interior dielectric constant was set to 1.0 and the outer dielectric constant was set to 80.0. The normal-mode analysis was performed to estimate the conformational entropy upon ligand binding using the nmode program [17,18]. In view of the high computational demand, only 40 snapshots from the last 10ns of the MD minimization simulation were used to calculate the entropy contribution, with a convergence of 0.0001 kcal mol^{-1} $Å^{-1}$. The cut-off value was set to 1000, and the dielectric constant was set to 4. The calculated ligand-receptor interaction energies in the complexes were partitioned on a per residue basis using the NAMD-energy module in VMD using the MD parameters. The binding interaction of each ligand-residue pair includes two terms: the vdW contribution (ΔG_{vdW}) and the electrostatic contribution (ΔG_{elec}). The two components were calculated using 2000 snapshots from the last 10 ns of MD minimization.

3. Results

3.1. Root-mean-square deviations and fluctuations

The MD trajectories of the WT and C1156Y mutant systems were generated. The atomic RMSDs of the protein structures were calculated from the starting structures as a function of time. The small RMSD fluctuation during the simulations indicates the protein stability over the entire trajectory chosen for the analysis (Supplementary Fig. S1A and B). All analyses have been performed over the last 10 ns to guarantee an investigation over a well thermalized system.

The main chain RMSFs calculated over the trajectories display similar fluctuation patterns for the WT and the C1156Y-mutated models. Supplementary Fig. S1C shows that a large part of the residues is characterized by fluctuations not higher than 2.0 Å, in addition to the random coil regions (1137–1144, 1213–1222, and 1280–1292) that exceed 3.5 Å. However, a relatively higher fluctuating region (loops 1122–1130 and 1153–1157) was observed in the C1156Y mutant protein.

3.2. Cross-correlations and PCA

The correlated motion between the different protein regions was examined. As described by the DCC map [19], which was calculated on the Cα atoms (Fig. 1A and B), a red spot represents a correlation of above 0.5 (absolute value) between the two Cα atoms. The panels indicate that both the WT and C1156Y-mutated ALK have high degrees of correlation. The maps of the two systems are distinct, and a higher degree of correlation is observed in the C1156Y mutant protein.

The PCA, or essential dynamics [20,21] has also been used to compare the correlation differences between the WT and C1156Y-mutated proteins. The analysis based on all the Cα atoms of the two proteins, indicates that approximately 80% of the motion depends on the first 30 eigenvectors that have the largest eigen values (Supplementary Fig. S2). The dynamical differences between the two systems can be observed by inspecting the Cα projections of the MD motions along the first eigenvector having 20% of the total motion (see Supplementary Fig. S2).

The projections of the motion are shown in Fig. 1C and D. The arrows indicate the direction of the motion, and the amplitude of the backbone motion goes from blue to red. In the mutant protein, the unique regions with relatively high mobilities are represented by loops 1122–1130 and 1153–1157 (Supplementary Movie S1). The different motions induce distinct residue behaviors during binding with crizotinib.

3.3. Hydrogen bond analysis

Hydrogen bonds are vital to ligand binding. The hydrogen bond analysis results indicate that the hydrogen bonds between M1199.H-Crizonib.N4 and E1197.O-Crizonib.H14 are retained in the C1156Y-mutated protein (Supplementary Fig. S3A and B). However, the introduction of a tyrosine in position 1156 weakens the hydrogen bond between crizotinib and Gly1123, resulting in an unstable hydrogen bond fluctuation (Supplementary Fig. S3C).

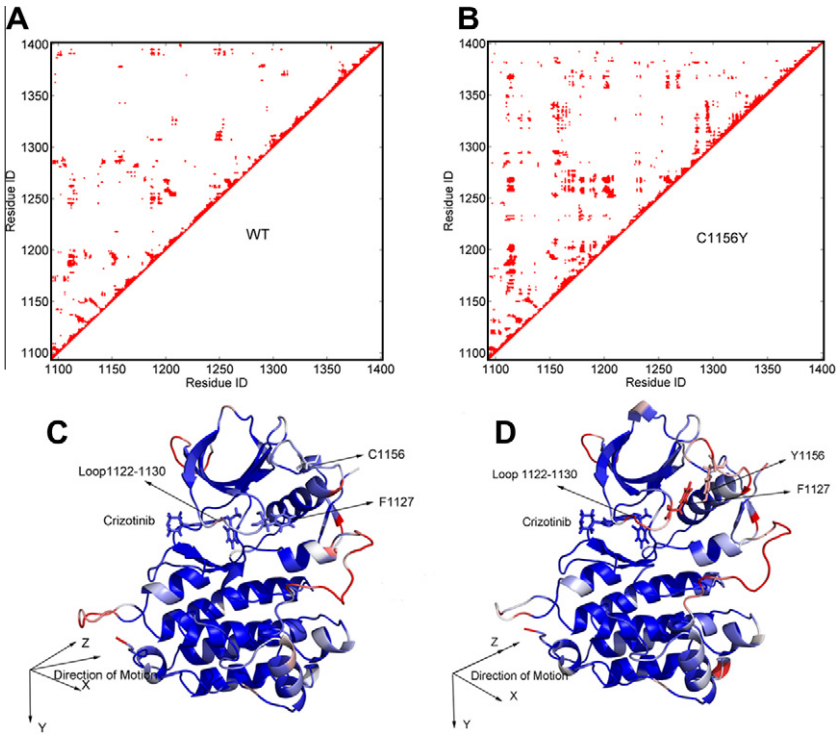

Fig. 1. Dynamic cross-correlation maps and the motion projections for two models. The red dots represent the Cα motion correlations with $|C_{ij}| \geqslant 0.5$ (C_{ij} is defined in Section 2) for the WT (A) and C1156Y-mutated (B) proteins. Ribbon representation of the motion projections along the first eigenvector for the WT complex (C) and the C1156Y-mutated protein (D). The arrows indicate the direction of the motion, and the amplitude of the backbone motion goes from blue to red. (For interpretation of the references to colour in this figure legend, the reader is referred to the web version of this article.)

3.4. Comparison of the structures of the WT and C1156Y models

To determine the effects of the C1156Y mutation, the average structure of the C1156Y model during the last 10 ns of the simulation was compared with that of the corresponding WT model. Crizotinib exhibited an RMSD value of 1.54 Å when the C1156Y model was fitted into the WT model. Fig. 2 shows that the C1156Y mutation caused conformational changes in the binding cavity even though it is far (approximately 15 Å) from the active site. C1156Y increased the interactions between Y1156 and F1127. Thus, loop 1122–1130 was pulled closer to Y1156, thereby inducing an approximately 2.9 Å conformational shift in loop 1122–1130. In

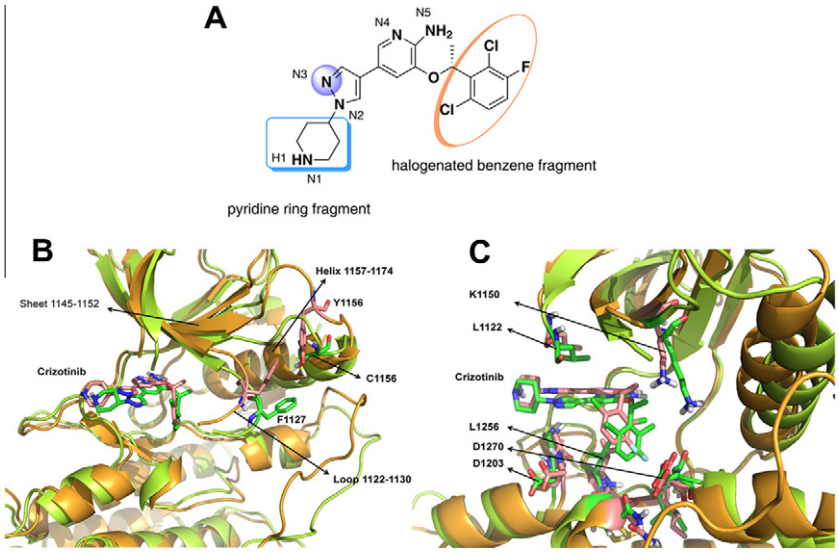

Fig. 2. Alignment of the average structures of the wild-type (green) and mutated (orange) ALK. (A) Chemical structure of crizotinib. Complexes structures (B and C) were obtained during the last 10 ns trajectory of MD. Crizotinib in the WT and mutated complexes is colored in green and pink respectively. (B) C1156Y results in marked conformational changes in loop 1122–1130, sheet 1145–1152, and helix 1157–1174. (C) The dislocation of crizotinib increased the distances with the residues at the active site, including G1202, D1203, N1254, C1255, L1256, I1268, G1269, and D1270. The images were created by PyMol (www.pymol.org).

Table 1
Calculated binding free energies of crizotinib complexed with the wild-type (WT) and the C1156Y mutant (C1156Y) ALK using MM/GBSA (kcal/mol).

Energy	WT	C1156Y
ΔE_{vdW}[a]	−48.11 ± 0.18[b]	−42.58 ± 0.15
ΔE_{elec}[c]	−17.08 ± 0.18	−14.79 ± 0.22
ΔG_{GB}[d]	32.98 ± 0.14	28.72 ± 0.15
ΔG_{solv}[e]	−5.48 ± 0.01	−4.96 ± 0.01
$\Delta G_{nonbonded}$[f]	−65.19 ± 0.25	−57.37 ± 0.24
$\Delta E_{Enthalpy}$[g]	−37.67 ± 0.17	−33.61 ± 0.16
$T\Delta S$[h]	−17.03 ± 1.18	−14.79 ± 1.29
ΔG_{bind}[i]	−20.66 ± 0.17	−18.82 ± 0.16

[a] Van der Waals energy.
[b] Standard error of the mean.
[c] Electrostatic energy.
[d] Electrostatic and nonpolar contribution to salvation.
[e] Electrostatic contribution to salvation.
[f] Non-bonded energy
[g] Binding free energy in the absence of entropic contribution.
[h] Entropic contribution.
[i] Binding free energy

addition, marked conformational changes in sheet 1145–1152 and helix 1157–1174 (approximately 2.7 and 2.8 Å for the largest Cα distance shift, respectively) were observed (Fig. 2B).

3.5. Crizotinib-ALK binding energy

MM/GBSA has been widely used in evaluating the interactions between ligands and receptors [22–24]. Hence, the effect of C1156Y on the binding energy was determined using MM/GBSA. The binding energies of crizotinib (Table 1) without considering the entropy ($\Delta E_{Enthalpy}$) are −37.67 and −33.61 kcal/mol. If the entropy contribution is included, the binding energies (ΔG_{bind}) are −20.66 and −18.82 kcal/mol, which are qualitatively consistent with $\Delta E_{Enthalpy}$. These results suggest that the binding affinity of crizotinib is less favorable in the mutant protein.

The nonbonded energy, which consists of vdW and electrostatic interactions contributed the most to the binding energy. Further inspection shows that the diminished vdW and electrostatic contributions in the C1156Y mutant were 5.53 and 2.29 kcal/mol, respectively, upon binding. Given that the nonbonded energy is critical to the stability of the ligand–receptor complex [25], the results indicate that C1156Y can attenuate the stability of the drug–target complex by decreasing the nonbonded interaction.

The binding free energy was decomposed into ligand residue pairs (Fig. 3) to gain a detailed picture of the binding energy. Each difference ($\Delta E = E_{C1156Y} - E_{WT}$) in ligand residue energy was calculated. A positive ΔE indicates a weaker binding affinity in the mutant protein, whereas a negative ΔE indicates a stronger binding affinity. The C1156Y mutation clearly weakened the nonbonded

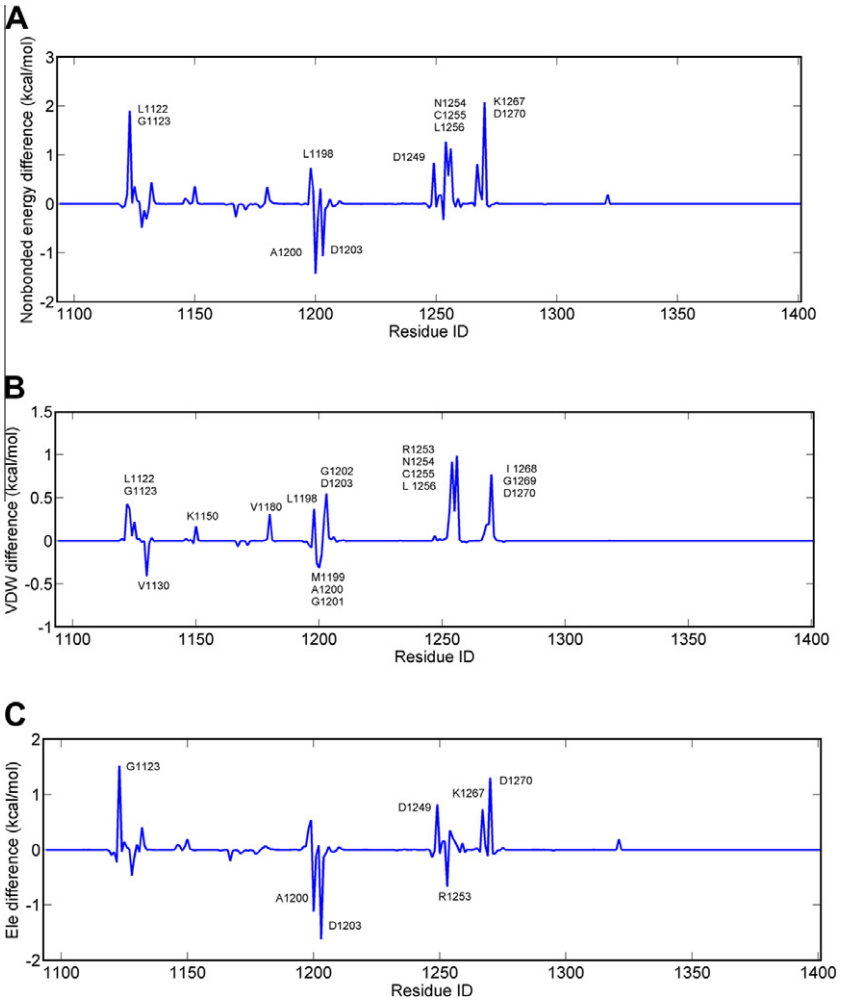

Fig. 3. Differences in contribution of residues to the binding energy between the wild-type and C1156Y mutant. $\Delta E = E_{C1156Y} - E_{WT}$; A positive ΔE indicates a weaker binding affinity in the mutant protein, whereas a negative ΔE indicates a stronger binding affinity. (A) nonbonded energy terms. (B) van der Waals terms (VDW). (C) electrostatic energy terms (Ele).

interactions of many of the ligand residue pairs with crizotinib (Fig. 3A) and reduced their binding affinities.

Fig. 3B shows a significant decrease in vdW interactions, including those in G1122, D1123, K1150, V1180, L1198, G1202, D1203, N1254, C1255, L1256, I1268, G1269, and D1270. To determine the reason for the decrease, the conformations of ALK were investigated in detail. The L1122, G1123, and K1150 residues were located in loop 1122–1130 and β-sheet 1145–1152 (Fig. 2C). However, the C1156Y mutation led to a shift in loop 1122–1130 and β-sheet 1145–1152, which resulted in the noticeable enlargement of the binding cavity as well as in the increased distances between the residues and crizotinib. Residues G1202, D1203, N1254, C1255, L1256, I1268, G1269, and D1270 are located at the active site and thus directly interact with crizotinib (Fig. 2C). Although the side chains of these residues show no evident deviations, the dislocation of crizotinib increased its distances with the residues, thereby decreasing the vdW interactions. By contrast, some of the residues, such as V1130, M1199, A1200, and G1201, strengthened the vdW interactions with crizotinib. Distance analyses demonstrate that the distance between atom CB in V1130 and atom Cα in crizotinib was reduced from 5.13 Å to 5.02 Å. Additionally, the pyridine ring of crizotinib is closer to residues M1199, A1200, and G1201 in the C1156Y model because of the displacement of crizotinib, thereby increasing the vdW interactions. However, the decreased vdW interactions were dominant in both the number of residues and the level of variation.

The difference in the electrostatic energies between the two models was also analyzed in terms of the energy loss in the electrostatic component of the C1156Y mutant. Fig. 3C shows a decrease in electrostatic interactions for G1123, D1249, K1267, and D1270, whereas an increase was observed for A1200, D1203, and R1253. Analysis of the conformations reveals that the shift in loop 1122–1130 and the dislocation of crizotinib were responsible for the phenomenon. On one hand, the shift in loop 1122–1130 increased the H-bond distance between the amide hydrogen atoms of G1123 and the N3 of crizotinib from 2.45 to 3.45 Å. On the other hand, the displacement of crizotinib, particularly the rotation of the halogenated benzene fragment (approximately 2 Å), increased the distances of crizotinib from residues D1249 (from 8.9 to 10.6 Å), D1270 (from 5.4 to 5.9 Å), and K1267 (from 6.1 to 7.6 Å), thereby weakening the electrostatic interactions. Therefore, the increased electrostatic interactions of residues A1200, D1203, and R1253 in the C1156Y model may be attributed to the dislocation of crizotinib. In contrast to the energy change in vdW (–1 to 0.5 kcal/mol), the electrostatic energy change was more prominent (–1.5 to 1.5 kcal/mol) (Fig. 3B and C). The increased electrostatic interactions markedly compensated for the effect of the decreased electrostatic interactions in the mutant protein. Thus, decreased vdW interactions play a dominant role in weakening the binding affinity to crizotinib.

4. Discussion

The results obtained from the MD simulations indicate that the two models fully maintained a stable structure over the whole simulation period. Our analyses demonstrate the dynamical differences between the WT and C1156Y-mutated proteins. After careful observations of the superimposed structures, three regions (loop 1122–1130, sheet 1145–1152, and helix 1157–1174) in the two models showed relatively large conformational differences. Compared with the WT complex, loop 1122–1130 in the mutated complex moved slightly away from the active site (closer to Y1156), and induced a partial structural rearrangement of sheet 1145–1152 and helix 1157–1174. The conformational changes in the regions also led to the positional adjustment of crizotinib.

The binding energy calculation indicates a weaker binding affinity for crizotinib in the C1156Y mutant. Further residue-inhibitor energy decomposition calculations indicate a decrease in both vdW and electrostatic interactions in the mutant protein upon binding. It appears vdW interactions appeared to have the largest contributions to the binding free energy. This result is attributed to the highly hydrophobic binding pocket of crizotinib. However, the magnitude of electrostatic contributions should also be considered. Differences in the electrostatic components between the WT and mutated complexes show an energy loss, which suggest the occurrence of unfavorable interactions due to the C11156Y mutation; this finding is consistent with the weakening of hydrogen bonds with crizotinib.

Consequently, this study indicates that the C1156Y mutation induces a dynamical perturbation as well as a partial structural rearrangement, which weakens the preferred interactions of crizotinib preshaped to the WT binding site. Shen et al. [6] proposed that the C1156Y mutation would indirectly lead to conformational changes in the active site. However, the current study reveals the occurrence of conformational changes in β-sheet 1145–1152 and α-helix 1157–1174 in addition to the changes in loop 1123–1130 mentioned by Shen et al.. Hence, the present study can provide a more comprehensive explanation for crizotinib resistance.

In summary, the mechanism of resistance caused by C1156Y has been clarified through MD simulations and binding energy calculations. Although the C1156 residue of ALK is located at the non-active site and thus has no direct interaction with crizotinib, the simulations indicate that C1156Y induces crizotinib displacement and affects the conformations of loop 1122–1131, β-sheet 1145–1152, and α-helix 1157–1174. These conformations cause a decline in the vdW and electrostatic interactions between crizotinib and ALK. The results of the present study reveal the detailed resistance mechanism of the C1156Y mutation at the non-active site, which may provide a clue for the design of new drugs to combat resistance caused by mutations.

Acknowledgments

This study was supported by the National Science Foundation for Post-doctoral Scientists of China (20110491166).

Appendix A. Supplementary data

Supplementary data associated with this article can be found, in the online version, at http://dx.doi.org/10.1016/j.bbrc.2012.05.120.

References

[1] A.S. Crystal, A.T. Shaw, New targets in advanced NSCLC: EML4-ALK, Clin. Adv. Hematol. Oncol. 9 (2011) 207–214.
[2] Cancer Statistics, A. Jemal, R. Siegel, J.-Q. Xu, et al., Cancer Statistics, 2010, CA Cancer J. Clin. 60 (2010) 277–300.
[3] M. Soda, Y.L. Choi, M. Enomoto, et al., Identification of the transforming EML4-ALK fusion gene in non-small-cell lung cancer, Nature 448 (2007) 561–566.
[4] B. Hallberg, R.H. Palmer, Crizotinib–latest champion in the cancer wars?, N Engl. J. Med. 363 (2010) 1760–1762.
[5] Y.L. Choi, M. Soda, Y. Yamashita, et al., EML4-ALK mutations in lung cancer that confer resistance to ALK inhibitors, N. Engl. J. Med. 363 (2010) 1734–1739.
[6] L. Shen, H.-F. Ji, More on crizotinib, N. Engl. J. Med. 364 (2011) 777–778.
[7] J.-J Cui, M. Tran-Dube, H. Shen, et al., Structure based drug design of crizotinib (PF-02341066), a potent and selective dual inhibitor of mesenchymal-epithelial transition factor (c-MET) kinase and anaplastic lymphoma kinase (ALK), J. Med. Chem. 54 (2011) 6342–6363.
[8] M.J. Frisch, G.W. Trucks, H.B. Schlegel, et al., Gaussian 03, Gaussian Inc., Wallingford, CT, 2004.
[9] C.I. Bayly, P. Cieplak, W.D. Cornell, et al., A well-behaved electrostatic potential based method using charge restraints for deriving atomic charges: the RESP model, J. Phys. Chem. 97 (1993) 10269–10280.
[10] V. Hornak, R. Abel, A. Okur, et al., Comparison of multiple Amber force fields and development of improved protein backbone parameters, Proteins 65 (2006) 712–725.

[11] J. Wang, R.M. Wolf, J.W. Caldwell, et al., Development and testing of a general amber force field, J. Comput. Chem. 25 (2004) 1157–1174.
[12] W.L. Jorgensen, J. Chandrasekhar, J.D. Madura, et al., Comparison of simple potential functions for simulating liquid water, J. Chem. Phys. 79 (1983) 926–935.
[13] T. Darden, D. York, L. Pedersen, Particle mesh Ewald: An N·Log(N) method for Ewald sums in large systems, J. Chem. Phys. 98 (1993) 10089–10092.
[14] J.C. Phillips, R. Braun, W. Wang, et al., Scalable molecular dynamics with NAMD, J. Comput. Chem. 26 (2005) 1781–1802.
[15] J.P. Ryckaert, G. Ciccotti, H.J.-C. Berendsen, Numerical integration of the cartesian equations of motion of a system with constraints: molecular dynamics of n-alkanes, J. Comput. Phys. 23 (1977) 327–334.
[16] A. Onufriev, D. Bashford, D.A. Case, Exploring protein native states and large-scale conformational changes with a modified generalized born model, Proteins 55 (2004) 383–394.
[17] J.C. Phillips, R. Braun, W. Wang, et al., The Amber biomolecular simulation programs, J. Comput. Chem. 26 (2005) 1668–1688.
[18] B. Brooks, M. Karplus, Harmonic dynamics of proteins: normal modes and fluctuations in bovine pancreatic trypsin inhibitor, Proc. Natl. Acad. Sci. USA 80 (1983) 6571–6575.
[19] J.A. McCammon, S.C. Harvey, Short time dynamics, in: Dynamics of proteins and nucleic acids, Cambridge University Press, 1987, pp. 79–116.
[20] A.E. Garcia, Large-amplitude nonlinear motions in proteins, Phys. Rev. Lett. 68 (1992) 2696–2699.
[21] A. Amadei, A.B. Linssen, H.J. Berendsen, Essential dynamics of proteins, Proteins 17 (1993) 412–425.
[22] T.-J. Hou, J.-M. Wang, Y.-Y. Li, et al., Assessing the performance of the MM/PBSA and MM/GBSA methods. The accuracy of binding free energy calculations based on molecular dynamics simulations, J. Chem. Inf. Model. 51 (2011) 69–82.
[23] G. Rastelli, A. Del Rio, G. Degliesposti, et al., Fast and accurate predictions of binding free energies using MM-PBSA and MM-GBSA, J. Comput. Chem. 31 (2010) 797–810.
[24] L. Xie, T. Evangelidis, P.E. Bourne, Drug discovery using chemical systems biology: weak inhibition of multiple kinases may contribute to the anti-cancer effect of nelfinavir, PLoS Comput. Biol. 7 (2011) e1002037.
[25] H. Lu, P.J. Tonge, Drug-target residence time: critical information for lead optimization, Curr. Opin. Chem. Biol. 14 (2010) 467–474.